Evidencing the Impact of Climate Change on the Phytoplankton Community of the Mediterranean Sea Through a Bioregionalization Approach

Roy El Hourany, Carlos Mejia, Ghaleb Faour, Michel Crépon, Sylvie Thiria

JGR Oceans

RESEARCH ARTICLE
10.1029/2020JC016808

Key Points:

- The Mediterranean Sea is partitioned in seven bioregions with a neural classifier using satellite Sea Surface Temperature and chlorophyll-*a* concentration (Chla) and mixed-layer depth Argo-float data
- Temperature is increasing while the Chla concentration remains constant through the 18 years studied period for each bioregion
- Satellite estimates show that diatom and nanoplankton dominance is decreasing while cyanobacteria are increasing during the 18 studied years

Correspondence to:
R. El Hourany,
roy.elhourany@locean-ipsl.upmc.fr

Citation:
El Hourany, R., Mejia, C., Faour, G., Crépon, M., & Thiria, S. (2021). Evidencing the impact of climate change on the phytoplankton community of the Mediterranean Sea through a bioregionalization approach. *Journal of Geophysical Research: Oceans*, *126*, e2020JC016808. https://doi.org/10.1029/2020JC016808

Received 17 SEP 2020
Accepted 25 MAR 2021

Evidencing the Impact of Climate Change on the Phytoplankton Community of the Mediterranean Sea Through a Bioregionalization Approach

Roy El Hourany[1], Carlos Mejia[2], Ghaleb Faour[3], Michel Crépon[2], and Sylvie Thiria[2,4]

[1]Institut de Biologie de l'Ecole Normale Supérieure (IBENS), Paris, France, [2]LOCEAN-IPSL, Paris, France, [3]National Center for Remote Sensing, CNRS-L, Beirut, Lebanon, [4]OVSQ, UVSQ, Versailles, France

Abstract We revisited the partitioning of the Mediterranean Sea into bioregions by processing satellite Sea Surface Temperature (SST) and Chlorophyll-*a* concentration (Chla) from ocean color observations combined with Argo mixed-layer depth for a period ranging from 2003 up to 2020. This regionalization was performed using an innovative classification based on self-organizing maps, the so-called 2S-SOM. We clustered the Mediterranean Sea waters into seven bioregions governed by specific physical and biogeochemical characteristics. We studied the interannual variability of these bioregions over the 18 years. We showed that the temperature is increasing with a mean rate of 0.4°C per decade. The chlorophyll-*a* concentration is quasi constant, but we evidenced a noticeable change in satellite-derived phytoplankton communities: Diatoms concentration is decreasing while cyanobacteria concentration is increasing. The bioregion trends could be related to global warming. The whole Mediterranean Sea is shifting to an eastern Mediterranean state.

Plain Language Summary The Mediterranean is a miniature ocean where most of the processes documented in the global ocean are encountered. At a regional scale, the Mediterranean Sea plays a role of sentinel with regards to global warming. Indeed, the Mediterranean Sea has shown a warming trend throughout several studies, but the primary production seems to be stable. In this study, we propose a new decomposition of the surface Mediterranean waters into bioregions based on a neural network classifier applied to satellite and Argo-float observations. The resultant bioregionalization shows a significant interannual variability and trends that coincide with the warming of the basin. Using satellite estimates of Phytoplankton groups, show significant changes in the phytoplankton community composition in every bioregion throughout the 18 years studied period. The bioregion trends could be related to global warming.

1. Introduction

The Mediterranean is a miniature ocean where most of the processes documented in the global ocean are encountered (Lejeusne et al., 2010). Indeed, important global features are present in it, but on smaller spatial and temporal scales (Bethoux et al., 1999) such as the thermohaline circulation forced by dense water formation in winter. In addition, several features of the Mediterranean make it a hotspot of marine biodiversity (Coll et al., 2010) and potentially vulnerable to climate change.

At regional scale, the Mediterranean Sea plays a role of sentinel with regard to global warming since it is very sensitive to climate change (Giorgi, 2006). Indeed, the Mediterranean Sea was one of the first ocean places where a warming trend was observed in the deep-water temperatures in the western basin and attributed to global warming (Bethoux et al., 1990). The Mediterranean Sea Surface Temperature (SST) has experienced an intensive and continuous warming since the mid-1980s, which is expected to increase throughout the 21st century under present climate scenarios (Somot et al., 2008). Several studies have shown an increase of the mean Mediterranean SST in the last three decades. Based on the 4 km Advanced Very High Resolution Radiometer (AVHRR) Pathfinder SST data set, Nykjaer (2009) estimated a mean warming trend of 0.03 ± 0.008°C/year in the western Mediterranean Sea and 0.05 ± 0.009°C/year in the eastern basin from 1985 to 2006. Similar results were found by (López García & Camarasa, 2011) from 1985 to 2007. Based on Reynolds' SST reanalysis (Reynolds et al., 2007), Shaltout and Omstedt (2014) found a mean warming trend of 0.035 ± 0.007°C/year during a 31-year period (1982–2012) over the Mediterranean Sea. And recently,

Pisano et al. (2020) highlighted a mean warming trend of 0.041 ± 0.006°C/year over the whole Mediterranean Sea from 1982 to 2018.

The increase of the Mediterranean SST modifies its vertical stratification and consequently the exchanges between the surface and the deeper layers. This incited us to study the surface warming impact on the phytoplankton and particularly on its distribution according to bioregions. It is therefore important to characterize the state of the Mediterranean Sea with robust estimators and then to study its long-term evolution. In this study, we address this problematic by introducing a new bioregionalization of the Mediterranean Sea based on neural network methods.

Regionalization is defined by specific physical conditions, chemical properties, and biological communities, which are homogeneous in each region we have defined. Since the 1990s, satellite remote sensing of phytoplankton chlorophyll-*a* (Chla) has made it possible to describe the dynamics of the phytoplankton and to delimit provinces at basin and global scales (Longhurst et al., 1995).

Longhurst (1998) described the Mediterranean as a specific region, without proposing sub-regions within the basin, despite its heterogeneity. Since then the regionalization of the Mediterranean has been the subject of many studies. Spalding et al. (2007) described the Mediterranean as a temperate province belonging to the North Atlantic domain. It has been subdivided into seven eco-regions: The Adriatic Sea, the Aegean Sea, the Levantine Basin, the Tunisian Plateau/Gulf of Sidra, the Ionian Sea, the Western Mediterranean, and the Alboran Sea. D'Ortenzio and Ribera d'Alcalà (2008) and Mayot et al. (2016) considered the phenology of phytoplankton; Nieblas et al. (2014) and Reygondeau et al. (2017) dealt with geochemical variables, such as temperature, salinity and nutrient concentration; Berline et al. (2014), Nieblas et al. (2014), and Rossi et al. (2014) considered the hydrodynamic properties of the basin's surface waters; Reygondeau et al. (2014) exploited the biological composition given by a modeling of marine species habitats in the basin.

The study of Reyngondeau et al. (2017) confirms that classical variables, such as SST, Chla, and mixed-layer depth (MLD) well describe the west-east gradient of the Mediterranean Sea and allow a coherent partitioning of surface waters. D'Ortenzio et al. (2020) extended the work of D'Ortenzio and Ribera d'Alcalà (2008) by incorporating observations of biogeochemical Argo floats to ocean color satellite observations. They found that the Argo floats observations are in good agreement with the partition in five bioregions done by D'Ortenzio and Ribera d'Alcalà (2008).

All these regionalization studies are issued from multivariate analysis of ocean data such as k-means analysis or Hierarchical Ascending Clustering (HAC). These methods have been shown to be efficient in defining coherent data patterns that can be related to the main oceanic features (D'Ortenzio & Ribera d'Alcalà, 2009; Foukal & Thomas, 2014; Yoder & Kennelly, 2003). Each method has its own drawbacks: The k-means algorithm must determine an a priori number of clusters (for computational efficiency this number must be limited), the HAC has difficulties when the number of patterns under study is too large. The Self-Organizing Maps (SOMs; Kohonen, 2013) is a useful alternative method which can be considered as an extension of the k-means; as an example in Basterretxea et al. (2018) the Mediterranean sea was clustered into bioregions using Chla satellite data and the SOM algorithm.

In this study, we used a modified Self-Organizing method, called 2S-SOM to provide a robust decomposition of the Mediterranean into bioregions using a well-documented set of variables (SST and Chla given by the satellite observations of MODIS Aqua; MLD from Argo floats in situ observations). The 2S-SOM has been proposed by Yala et al. (2020) to retrieve phytoplankton pigment concentration from ocean color satellite data. The 2S-SOM algorithm differs from the classical SOM algorithm by introducing, during the learning phase, a system of weights acting on the most sensitive variables. The use of this type of algorithm offers the advantage of taking the existing relationships between the variables into account, to consider the non-linear relationships among the variables at regional scale and to provide the weights associated with the variables during the learning phase according to their geographical location in the Mediterranean Sea. Once the regionalization via 2S-SOM is made, it is possible to evaluate the interannual variability and calculate trends during the study period from 2003 till 2020.

The study is articulated as follows: In Section 2, we present the data we used (in situ and remote sensing observations). The principle of the clustering method (2S-SOM) is given in Section 3. The statistical results

of the method are presented in Section 4. In Section 5, we analyze the different bioregions. In Section 6, we study the interannual variability and the trends of the bioregions. Interannual variabilities and trends of phytoplankton composition in the Mediterranean Bioregions are discussed in Section 7. A conclusion is presented in Section 8.

2. Databases

In the following, we present the satellite and in situ measurements we processed.

2.1. Satellite Data

Chla and SST are based on the MODIS-Aqua averaged products over an 18-year period (2003–2020). This monthly climatology data was downloaded from the ocean color portal (oceancolor.gsfc.nasa.gov), with a resolution of 4 km. By default, these variables were calculated by specific algorithms described in the following.

2.1.1. Chlorophyll-*a*

Chla is calculated by an empirical relationship derived from in situ Chla measurements and marine reflectance (*Rrs*) in the blue-green region of the visible spectrum. The current implementation of the Chla algorithm uses the default OC3M algorithm for the MODIS sensor (Campbell & Feng, 2005), merged with the *CI* algorithm (color index of Hu et al., 2012). The use of such an algorithm is restricted to relatively clear water, and its contribution is to reduce artefacts and bias in the estimation of Chla in these waters (Hu et al., 2012).

The Chla concentration is estimated with the *CI* algorithm for concentrations less than 0.15 mg m^{-3}; for concentrations greater than 0.2 mg m^{-3}, the OC3M algorithm is used. Between these two values, the *CI* and OC3M algorithms are merged by weighted averages.

2.1.2. Sea Surface Temperature

The algorithm used for calculating the SST is based on a modified version of the (Walton et al., 1998) algorithm, most recently described in Kilpatrick et al. (2015). The use of this algorithm provides product continuity between NASA's current and future infra-red sensors and heritage Pathfinder SST from AVHRRs, thus enabling the generation of a 30+ year record of space-based measurements of SST from satellites.

2.2. Mixed-Layer Depth Climatology Data

The Mediterranean monthly MLD climatology data was extracted from the global monthly MLD climatology data (Holte et al., 2017; http://mixedlayer.ucsd.edu/) which consists of 1.5M Argo temperature profile measurements made between January 2000 and April 2018 and processed using a method described by Holte and Talley (2009) in order to obtain the MLD. The monthly MLD climatology is then determined by clustering the MLD values into 1° × 1° boxes and averaging for each month over the 18 years.

2.3. Learning Database, *D*

The study area is delineated by the following geographic coordinates: 46.5°N, 30°N, and 7.5°W, 36°E. To each ocean pixel of this zone corresponds 12-monthly values of Chla, SST, and MLD averaged over the duration of the study period (2003–2020).

The MLD is averaged in boxes of (1° × 1°) which is a limitation to a fine study of the Mediterranean Sea; a monthly image of MLD on the Mediterranean is composed of $56 \times 17 = 952$ boxes, while that of Chla or SST is $1{,}081 \times 397 = 429{,}157$ pixels. Each MLD box is therefore associated with Chla and SST values averaged on the MLD boxes.

Therefore, the final database ($\boldsymbol{D}$) gathers the three variables (Chla, SST, and MLD) in boxes of 1° × 1° covering the Mediterranean Sea and averaged at a monthly rate. It consists of a matrix of dimension $952 \times (12 \times 3)$ where each line (among the 952) corresponds to a box of the studied region, and the 36 columns are the variables; that is, 12-monthly climatology of Chla, SST, and MLD.

The monthly climatology of these three variables (SST, Chla, and MLD) constitutes the signature of the physical and biochemical processes which characterize oceanic regions having well defined specificities. The classification presented in this study tackles this problem by using a specific topological map: The 2S-SOM. Indeed, $\boldsymbol{D}$ consists of three blocks of variables, each one being the signature of specific phenomena. The learning phase of 2S-SOM allows the determination of the weights that spatially modify the importance of each block in the classification.

3. Methodology

3.1. The Bioregionalization Procedure

We used the 2S-SOM algorithm (Outtara, 2014; Yala et al., 2020), which is a modified version of the SOMs (Kohonen, 2013). The SOMs are unsupervised neural network classifiers, which have been commonly used to solve environmental problems (El Hourany, Abboud-Abi Saab, Faour, Aumont, et al., 2019; El Hourany, Abboud-Abi Saab, Faour, Mejia, et al., 2019; Jouini et al., 2013, 2016; Liu & Weisberg, 2005; Liu et al., 2006; Niang et al., 2003, 2006; Richardson et al., 2003). The SOM is structured in two layers. The first layer, which is the input layer, receives the vectors $\boldsymbol{z}_i \in \mathbb{R}^N$ of the multivariate data set $\boldsymbol{D}$ we want to cluster. The second layer is a rectangular neural grid with m neurons. Each neuron c is associated with a reference vector $\boldsymbol{w}_c$ characterizing a subset of $\boldsymbol{D}$ that gathers data having common statistical characteristics (usually not linear). The objective of the SOM is hence to compress the information contained in the multivariate set $\boldsymbol{D}$ by producing a small number m of reference vectors $\boldsymbol{w}_c$, which are statistically representative of $\boldsymbol{D}$. Each data is not too different of its nearest referent according to a distance (The Euclidean distance for the basic SOM algorithm). The number of neurons determines the granularity of the mapping, which in turn is responsible for the accuracy and the SOM map's generalization capabilities. A fundamental property of a SOM is the topological ordering provided at the end of the clustering phase: Close neurons on the map represent data that are close in the data space. The estimation of the referent vectors $\boldsymbol{w}_c$ of a SOM and the topological order is achieved through an iterative learning process consisting in minimizing a specific nonlinear cost function as in the K-Means algorithm. The number of neurons is determined empirically from solutions of similar problems and then adjusted, as described in Badran et al. (2005). The number of referents, that is the number of neurons, does not really matter because this number will be reduced into a small number of classes by using the HAC; we denote SOM + HAC this procedure.

When dealing with environmental data, the exact number of classes at the end of the SOM + HAC procedure is not known a priori. This number is determined at the end of the study by looking at the HAC dendrogram, which suggests several possibilities for the number of classes to estimate. When the SOM (or the 2S-SOM) is used for vector quantization, the number of neurons is large, and each neuron is dedicated to a small geographic area. A compromise between the number of classes that can be explained from a physical point of view and the number needed to include the information embedded in the data set is made. This procedure has been used with success in several papers (Farikou et al., 2015; Jouini et al., 2016; Niang et al., 2003; Sawadogo et al., 2009).

In the present study, we used the 2S-SOM + HAC procedure which consists in substituting the SOM with another more power-full Self-Organizing algorithm, the 2S-SOM, which is designed to take variables of different nature into account. In what follows, we used a simplified version of the 2S-SOM in which the variables are gathered in blocks of environmental variables having specific attributions. Indeed, the underlying assumption is that different geophysical phenomena appear depending on the geographic location. Consequently, the importance of an environmental variable varies from one location to another. In the 2S-SOM, the neurons collect data so that the relative influence of each environmental variable is considered through a set of weights. The block weighting facilitates the clustering procedure by considering the most relevant environmental variables for each cluster (or neuron). The different weights are estimated during the learning phase by minimizing a cost function similar to this used in the SOM estimation where, in addition to the classical cost, the entropy of each cluster is minimized (a complete presentation of the 2S-SOM can be found in Yala et al., 2020). We note that the weight attributed to every block of variable varies from one neuron c to another. The 2S-SOM can deal with a large quantity of variables and consequently of phenomena

embedded in these variables, choosing those that are the most significant for a given cluster and neutralizing those which are the least significant.

3.2. Implementation of the 2S-SOM

The learning database $\boldsymbol{D}$ is constituted of 952 boxes representing the Mediterranean Sea, each box being characterized by a vector $\boldsymbol{z_i}$ composed of the 12-monthly climatology of Chla, SST, and MLD, respectively, computed over the studied period. Each vector $\boldsymbol{z_i}$ is divided in three homogeneous blocks corresponding to the three climatology of the environmental variables we classify. The block weighting facilitates this classification by considering the most pertinent environmental block of variables on each cluster (or neuron). During the learning phase, the 2S-SOM takes advantage of the structuring of $\boldsymbol{D}$ into blocks and allows to distinguish the different influence of each climatology variable for each neuron corresponding to a specific geographical location. The 12 Chla monthly climatology values are $\log_{10}$ transformed, to better take the variability of low Chla values with respect to the high ones into account. The variables are then normalized by their variances, which homogenizes the range of variability of the different variables, and consequently facilitates the learning of the 2S-SOM.

We followed the algorithm implementation described in Ouattara (2014) and Yala et al. (2020); we trained 80 different 2S-SOM rectangular maps of size 10×5 and chose the one that minimizes the within-group variance at best.

We partitioned the variables in three blocks, one comprising the 12 Chla monthly values, the second one, the 12 SST monthly values, and the third one, the 12 MLD monthly values. This block partition permits a better determination of the influence of each environmental block of variables (j) on the classification with respect to the geographical location. For each neuron c, the weights α_{jc} ($j = 1, 2, 3$, $c = 1, 2, ..., 50$) attributed to each block of variables are determined during the learning phase (Yala et al., 2020). We note that the values of α_{jc} vary between 0 and 1 by construction and that $\sum_{j=1}^{3} \alpha_{jc} = 1$. The α_{jc} allow to consider the percentage of importance of each variable in the constitution of the boxes assigned to a given neuron.

4. Results

4.1. Analysis of the 2S-SOM-Med

As mentioned above, the referent vectors $\boldsymbol{w_c}$ are statistically representative of the data set $\boldsymbol{D}$. Figure 1 shows the components of the referent vectors associated with the neurons of the 2S-SOM for January, April, July, and October. The neurons are well organized. Each month evidences different gradients of Chla, SST, and MLD. Chla maxima are reached in January for the lower half of the 2S-SOM map and in April for the second upper half. Second, the SST shows a positive gradient from top to bottom of the neural map. All neurons recorded a maximum of SST in summer (represented by July in Figure 1) and this with a heterogeneous intensity reflecting a certain geographical regionalization of the data. The MLD presents a positive gradient from right to left with all neuron reaching their maximum of MLD in January. By analyzing the different arrangements of the variables in the 2S-SOM, relationships can be highlighted qualitatively; in winter, the MLD reaches maximum values that coincide with the high values of Chla and low SST; whilst in summer, the high values of SST coincide with low values of MLD and Chla.

4.2. Block Weight Analysis

Figure 2 shows the different weights α_{jc} assigned to the blocks of variables for every neuron of the 2S-SOM-Med map. For a given neuron, the sum of its weights (one for each block) is equal to 1. Note that, at the end of the training, the weights were distributed heterogeneously on the 2S-SOM-Med. Neurons attributed with a weight close to 1 for a given variable, represent geographical areas where this variable is highly significant for the classification.

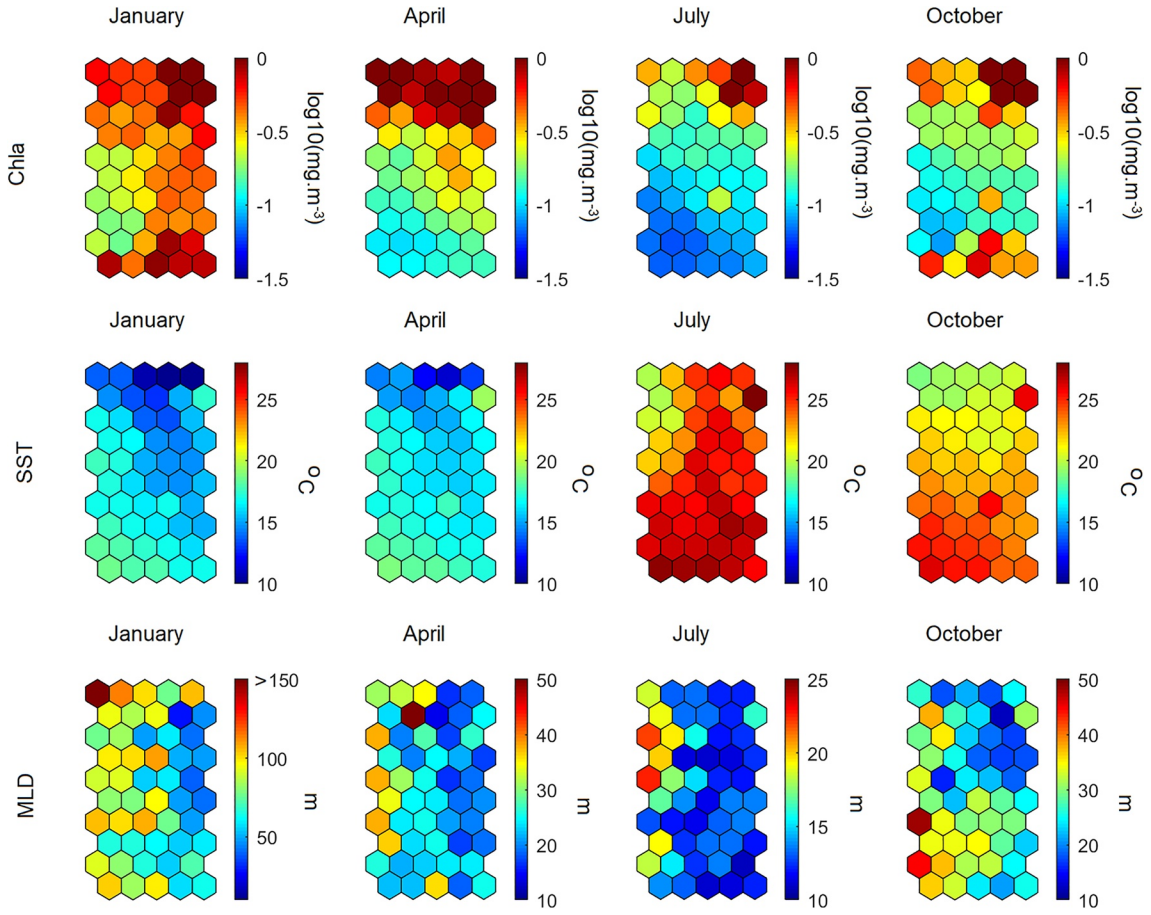

Figure 1. Values of Chla, SST, MLD inscribed by the 2S-SOM map for four months, showing the seasonal variation of the variables. The scale for the MLD varies according to the season. Chla, chlorophyll-*a*; MLD, mixed-layer depth; SOM, Self-Organizing Map; SST, Sea Surface Temperature.

At the end of this first analysis, we applied a HAC algorithm (Jain & Dubes, 1988) to regroup the neurons into a smaller number of classes which can be easily interpreted in terms of biogeochemical and physical processes. On the other hand, the assignation of neurons to a smaller number of classes allows to further analyze the α_{jc} weights distribution for each class.

4.3. Classification of Neurons

The HAC algorithm clustered the 2S-SOM-Med neurons into seven well separated classes (Figure 3). This number of classes was selected by choosing the most significant discriminative partition with respect to the full dendrogram of the HAC. The classification of the neurons of the 2S-SOM map and the representation of the block weight distribution associated with these neurons (one weight for each neuron) in each class are shown in Figure 2, respectively. The seven classes are well delineated, highlighting the good organization of the 2S-SOM-Med. More precisely, we can describe the different classes using the mean weight (see Table 1) estimated during learning in the following manner:

- Class 1 is characterized by important weights on MLD and SST, Chla playing an insignificant role
- Class 2 is characterized by strong MLD weights
- Classes 3 and 4 are characterized by strong SST weights
- Classes 6 and 7 are characterized by high Chla weights

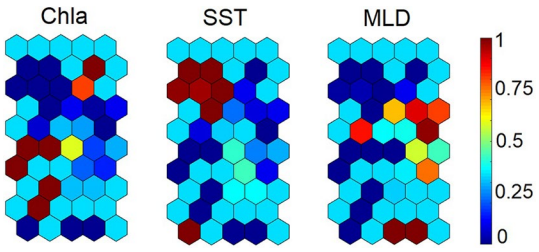

Figure 2. Weights α of the neurons represented on the 2S-SOM-Med map. SOM, Self-Organizing Map.

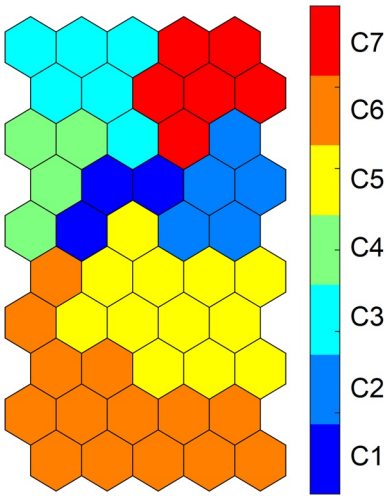

Figure 3. Representation of the 7 classes on the 2S-SOM-Med map. SOM, Self-Organizing Map.

4.4. Analysis of the Monthly Climatology of the Three Variables in the Different Classes

Figure 4 shows the geographic location of the 7 classes and Table 2 presentes the surface occupation of each bioregion calculated in number of pixels, Area (km^2) and percentage compared to the whole Med. The boxes belonging to a class are geographically contiguous. The 2S-SOM + HAC algorithm defines homogeneous regions whose characteristics mainly vary along the west-east axis of the Mediterranean Sea.

Except for class 7, the variables are well correlated inside every class in agreement with the homogeneity of the classes. The Spearman correlation was estimated for the three possible pairs of variables (Chla/SST, Chla/MLD, and SST/MLD) within each class and for the whole Mediterranean Sea (denoted whole Med in the following). Table 3 shows that the decomposition of the Mediterranean Sea in regions impacts the correlations. The three correlation module values are significantly higher for the pairs of variables in the C1...C6 regions than those for the whole Med. This is mainly because of the small correlation modules of C7. We note that the Chla/MLD correlation module, which is quite small for the whole Med, is significant for the regions C1 to C6 in agreement with the Chla/SST and SST/MLD high correlation values. C7, which is an atypical region, shows smaller correlations than those for the whole Med. This is due to the large diversity of the waters forming C7, which include waters flowing along the coast, influenced by the discharge of rivers (Nile, Po, and Rhone rivers) on the one hand (El Hourany et al., 2017; Lavender et al., 2009; McCall, 2008), shallow waters of the Gulf of Tunisia and in the Northern part of the Adriatic Sea, which are polluted by resuspended materials coming from the bottom on the other hand (Armi et al., 2010; Ferrara & Maserti, 1992; Raicich, 1996; Salem et al., 2015; Wang et al., 2007). This large diversity of variables affecting the quality of C7 waters leads to an important variability of Chla concentration which can explain the small correlation between Chla/SST and Chla/MLD (El Hourany et al., 2017).

We then analyzed the monthly climatological cycles corresponding to each class with respect to the three variables for the 18-year period. Figure 5 shows the climatological cycles and the associated box plots computed from the climatological cycle of the different geographical boxes constituting each class. In the last column, we illustrated the monthly climatology of Chla, SST, and MLD for the whole Med. We note a well-marked seasonal variability. We performed statistical tests to determine whether the climatological cycles of the seven classes are different from this of the whole Med. We compared the climatological cycle of each variable within each class to the corresponding climatological cycle of the whole Med by using ANOVA tests with confidence limits of 1% and 5%. In Figure 5, for each variable (Chla, SST, and MLD), the stars denote the classes for which a climatological cycle presents a significant difference from that of the whole Med. The arrow above each box plot denotes, for each month, a significant difference with respect to the same month of the whole Med (*red* arrow stands for a confidence limit <1% and *dark* arrow for a confidence limit <5%).

Table 1
Average α Weights with Respect to Classes and Variables

	Chla	SST	MLD
C1	0.06	0.44	0.51
C2	0.15	0.17	0.68
C3	0.17	0.67	0.17
C4	0.17	0.65	0.18
C5	0.36	0.29	0.35
C6	0.45	0.24	0.31
C7	0.52	0.24	0.24

The gray color highlights which parameter, among Chla, SST and MLD, contributed the most to the delimitation of the cluster (C1...C7).

Abbreviations: Chla, chlorophyll-*a*; MLD, mixed-layer depth; SST, Sea Surface Temperature.

5. Physical Analysis of the Seven Bioregions

The 2S-SOM algorithm provided a classification which is pertinent since the boxes belonging to a class are geographically contiguous and define homogeneous and non-pixelated regions. The MLD, SST, and Chla associated with a class have coherent annual cycles (Figure 5).

The Mediterranean Sea presents a well-marked seasonal cycle. SST is minimum in Winter (February, March) and maximum in summer (August, September) whilst Chla and MLD are minimum in summer and maximum winter. Except for class 7, which is atypical, Chla and MLD are anti-correlated with SST (see Table 3) which is a consequence of convection in the surface layers in winter (Somot et al., 2018). The dissimilarities between the classes can be explained by physical factors and air sea

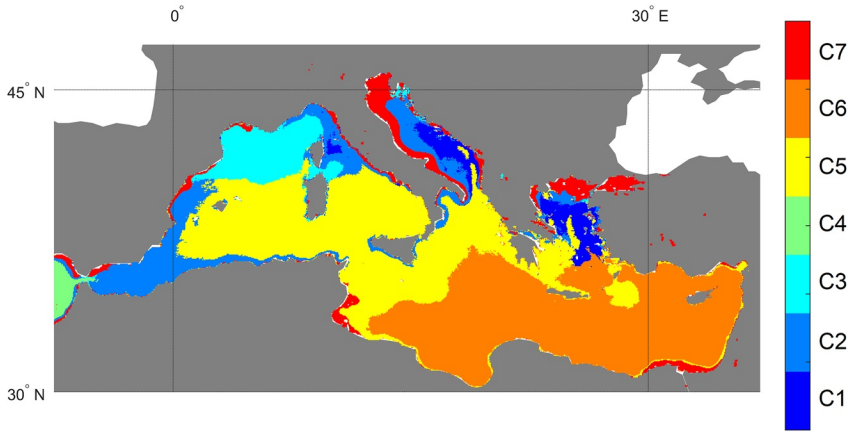

Figure 4. Geographic location of the 7 classes following 2S-SOM and HAC classification. HAC, Hierarchical Ascending Clustering; SOM, Self-Organizing Map.

exchange forcing: The most significant difference with the whole Med behavior is encountered for C3 (Liguro-Provençal basin and adjacent Balearic Sea) where the cycles of the three variables differ from those of the whole Med. In C3, Chla increases sharply in February–April, following a winter period of deep MLD and low SST resulting from deep winter convection which enriches the surface layers with nutrients.

C5 (respectively C6) occupies the largest surface of the western (eastern) Mediterranean Sea. C5 has a lower SST and a higher Chla concentration than those of C6. The western basin is strongly influenced by the fresh and warm Atlantic waters which inflow through the strait of Gibraltar. C6 occupies the eastern basin which is very warm with respect to the other classes and consequently oligotrophic (Tsiola et al., 2016) with a strong summer stratification and a shallow MLD. The cyclonic Rhodes gyre, which is located between Crete and Cyprus, is characterized by an intense winter convection with Ligurian Intermediate Water (LIW) formation that fills the intermediate depths of the eastern basin. This convection generates a cooling of the surface waters and an enrichment in nutrients, which causes an increased phytoplankton production, explaining why the Rhodes gyre belongs to C5 rather than C6.

C2 is present in several regions which are geographically disconnected: In the Alboran Sea, along the southern Spanish coast, then along the Moroccan, Algerian and Tunisian coasts advected by the Algerian current. C2 is also encountered in the central Adriatic flowing towards the Ionian Sea and in the northern Tyrrhenian Sea off the coasts of Italy and France. We also note the presence of C2 waters in the northern part of the Aegean Sea.

C7 includes coastal areas, such as those encountered along the east coast (Adriatic) and west of Italy (Tyrrhenian), part of the coast of the Gulf of Lion, and the coasts of Egypt and Lebanon. C7 waters are strongly influenced by river discharge, notably from the river Rhône and the Ebro (Syvitski & Saito, 2007), the Nile (Shata & El Fayoumy, 1970), and by human activities. C7 waters are also found in shallow areas where the tide is intense and re-suspends sediments (the Gulf of Gabes, the northern Adriatic Sea, and the Sea of Marmara). The SST seasonal cycle has a high amplitude, the minimum being about 10°C in February and the maximum 25°C, in August. The MLD is shallow in summer and can reach important values during winter due to mixing. One observes a large number of outliers for the three variables. This class is characterized by high Chla concentration reaching up to 2 mg m^{-3} during winter-spring and presenting low values during summer.

C1 is similar to the mean behavior of the whole Med; it regroups areas with low Chla concentration and a pronounced SST seasonal cycle. The MLD presents a seasonal cycle characterized by important values up to several hundred meters in January, February, and March, and is very shallow in August and to September. C1 waters are mainly found in the

Table 2
Surface Occupation of Each Bioregion Calculated in Number of Pixels, Area (km^2) and Percentage Compared to the Whole Med

	#Pixels	Area (*10^{-3} km^2)	Percentage of the whole Med
C1	6,166	98.65	4.01
C2	18,052	288.83	11.73
C3	10,020	160.32	6.51
C4	1,925	30.8	-
C5	53,632	858.11	34.84
C6	56,204	899.26	36.51
C7	9,852	157.63	6.40

Since C4 represents Atlantic Waters, this bioregion was neglected in the calculations of the percentages.

Table 3
Spearman Correlations of the Climatological Cycles Computed for the Mediterranean Sea and the 7 Classes

	Chla/SST	Chla/MLD	SST/MLD
Whole Med	-0.62	0.42	-0.68
C1	-0.77	0.69	-0.84
C2	-0.81	0.75	-0.85
C3	-0.77	0.66	-0.87
C4	-0.84	0.63	-0.68
C5	-0.82	0.74	-0.71
C6	-0.64	0.61	-0.69
C7	-0.36	0.33	-0.64

Abbreviations: Chla, chlorophyll-*a*; MLD, mixed-layer depth; SST, Sea Surface Temperature.

central Adriatic Sea and the Aegean Sea. These areas are subject to winter convection leading to Adriatic water formation on the one hand and LIW on the other hand.

C4 characterizes the Atlantic surface water of the Gulf of Cadiz and is observed in the Strait of Gibraltar forming a small tongue entering the Mediterranean.

5.1. Refining the Bioregions

Some atypical clusters could not have been detected through this procedure due to some subjectivity in cutting the branches of the connection tree associated with the HAC algorithm as discussed in Mignot et al. (2020). As an example, the 2S-SOM allows to refine the classification of C2 waters which presents well-marked spatial discontinuities. We showed that the neurons which constitute C2 (neurons 34-35, 43-44-45 in Figure 4) are associated with specific area of the Mediterranean Sea (Figure 6). The Alboran Sea and the Algerian Current are associated with neurons 43 and 44; the south-western part of the Balearic Sea,

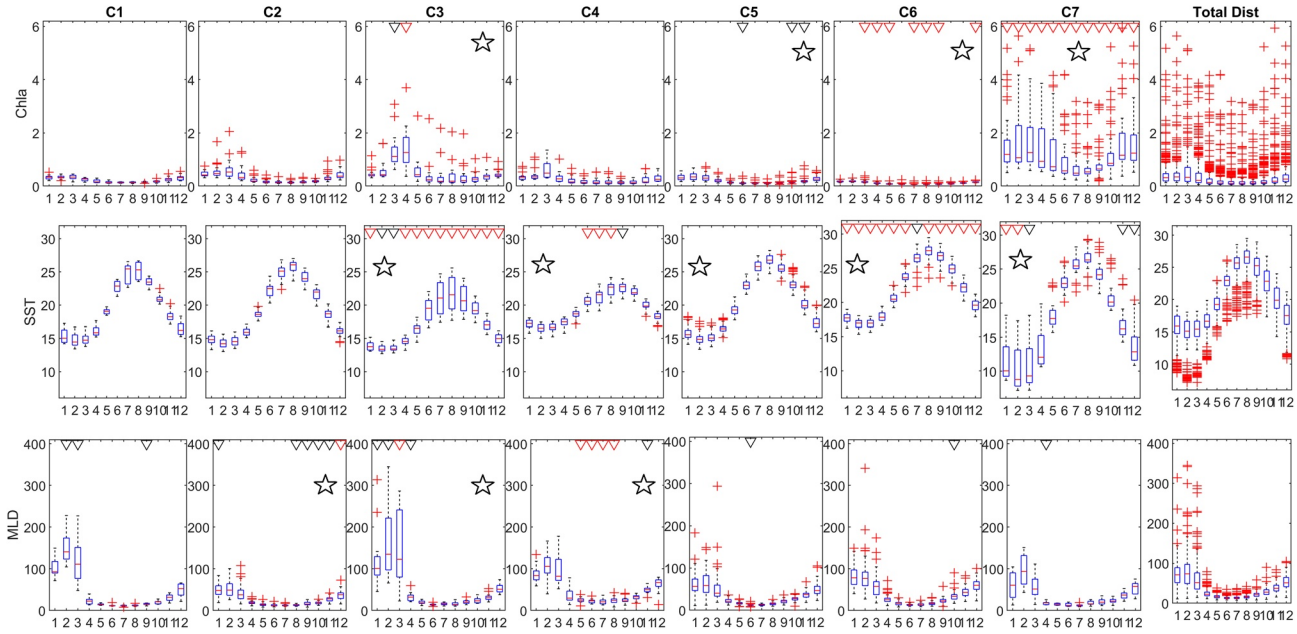

Figure 5. Monthly climatological cycles of the seven different classes and for the whole Med for the different variables and the associated box plots showing the variability extent. The box plots give the median, the first and last quartiles (respectively deciles); the red crosses represent the outliers.

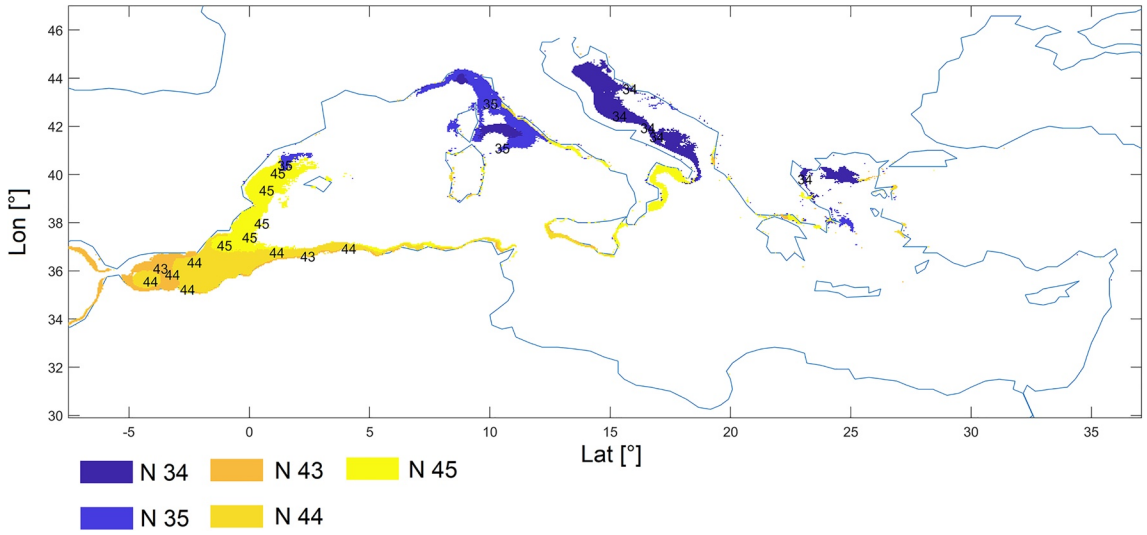

Figure 6. Neuronal decomposition of C2, showing the geographical areas associated with the different neurons forming this class.

with neuron 45; the eastern part of the Ligurian Sea, with neuron 35; and the center of Adriatic Sea and the north western part of the Aegean Sea, with neuron 34. Moreover, the waters observed along the south coast of Sicily are also associated with neuron 44, but they are colder than the Adriatic Sea waters and saltier than the Algerian current waters generating a quasi-permanent sharp North- South gradient of temperature and Chla across the strait. They correspond to a coastal upwelling generated by the thermohaline circulation forced by the density gradients between the Ionian Sea and the Tyrrhenian Sea, as argued by Jouini et al. (2016). They are constituted of salty and cold deep LIW coming from intermediate depths of the eastern Mediterranean basin and penetrating the western basin.

We were thus able to partition the C2 waters in different subclasses without any additional variable up to a certain limit for which additional variables, such as the salinity in the present case, should be necessary.

5.2. Comparison With Previously Proposed Bioregionalization

Several recent studies have proposed an objective regionalization of the Mediterranean Sea by using statistical clustering methods applied to various oceanic variables.

D'Ortenzio and Ribera d'Alcalà (2009), Mayot et al. (2016), Palmiéri (2014), and Uitz et al., (2012) focused their interest on phytoplankton phenology; Nieblas et al. (2014) and Reygondeau et al. (2017) used climatological averages of key biogeochemical variables (such as temperature, salinity, and nutrient concentrations); Berline et al. (2014), Nieblas et al. (2014), and Rossi et al. (2014) used the hydrodynamical properties of surface water masses; Reygondeau et al. (2014) used the composition of biological communities, inferred from the modeled habitats of marine species over the basin.

In the present study, we subdivided the Mediterranean Sea into 7 bioregions using satellite and Argo observations of classical oceanic variables (SST, MLD, and Chla). When comparing the bioregionalization obtained with the previous studies, we observe similarities but also some differences.

We have identified regions which are homogeneous and present coherent hydrodynamic, biogeochemical, and ecological features. The Liguro-Provençal Basin and the Balearic Sea (C3), the West Alboran Sea (C2), the Levantin Sea (C6), the Aegean and the Adriatic Sea (C1) were also identified as bioregions by Berline et al. (2014), D'Ortenzio and Ribera d'Alcalà (2009), Mayot et al., (2016), Nieblas et al. (2014), Palmiéri (2014), Reygondeau et al. (2014, 2017), and Rossi et al. (2014). This agreement in the statistical delimitation of these bioregions highlights their specificity regarding the hydrodynamic and biogeochemical variables. This congruence suggests that the observed physical parameters explain a significant part of the partition of hydrological and ecological variables at basin scale, which is based on homogeneous environmental conditions and well-marked gradients (Nieblas et al., 2014).

However, the dissimilarities correspond to areas whose boundaries present marked differences in the regionalization studies, depending on the variables considered. These areas of scattered frontiers are found within the Alboran Sea, the Tyrrhenian Sea, the western Algerian Sea, and the western Levantine Sea. Contrary to the homogeneous bioregions, these regions present some spatial variability and characterized by gradients of hydrological and biogeochemical conditions associated with a highly variable hydrography (d'Ovidio et al., 2004).

We can argue that the delimitation of the bioregions is due to an arbitrary choice regarding the variables considered, the clustering algorithms, and the cutoff level chosen in each study. This was already recognized in Ayata et al. (2018), by introducing a synthetic and contiguous consensus of bioregion partition for the Mediterranean Sea.

6. Interannual Variability and Trends of the Bioregions

The bioregions shown in Figure 4 represents the average state of the Mediterranean Sea from 2003 up to 2020. Due to the high discrimination properties of the 2S-SOM algorithm, we were able to monitor the interannual variability of the bioregions using yearly SST and Chla data.

We monitored the interannual variability of the bioregions by processing the monthly SST and Chla data with the 2S-SOM + HAC algorithms whose parameters were estimated in Section 3. As we do not have enough monthly MLD observations to cover the 2003–2020 period within every bioregion, we did not consider this parameter in this process. The 2S-SOM, like the SOM algorithm, can deal with missing data (El Hourany, Abboud-Abi Saab, Faour, Aumont, et al., 2019; Jouini et al., 2013; Yala et al., 2020) and is able to assign the available variables to a class using a truncated distance. The twelve monthly satellite values (Chla + SST) of each pixel of the Mediterranean for a year are assigned to a neuron (or a class corresponding to a bioregion) of the 2S-SOM + HAC algorithm according to the procedure defined in Section 3 using the truncated distance. The Mediterranean is thus partitioned in bioregions for every year between 2003 and 2020 (Figure 7).

The yearly spatial patterns of the seven classes are consistent with the patterns found for the 2003–2020 climatology shown in Figure 4, but they exhibit some interannual variability of their surface extent. Following that, we estimated the yearly trends of the SST, the Chla, and the bioregion extent over the studied period 2003–2020.

We estimated the yearly trends of every bioregion extent over the 2003–2020 period by computing the percentage of pixels that they occupy in the Mediterranean. A linear fit model was then applied to estimate the yearly trend. Concerning the SST and Chla data trends, we computed monthly anomalies by subtracting the monthly climatology to the monthly values. This procedure eliminates the seasonal signal. A linear fit model was then performed to estimate the yearly trend. The significance of the trends was evaluated using a Mann-Kendall test (Colella et al., 2016). This latter is a non-parametric test that characterizes the trend of a series of data, whether it is consistently increasing or decreasing (monotonically) or non-existent.

The surface extent of the two largest classes C5 and C6 increase over the studied period at a yearly rate of 0.36% ± 0.14 and 0.48% ± 0.09, respectively, while C3 and C2 surface extent decrease at a yearly rate of −0.19% ± 0.09 (Table 4 and Figure 8). We note that the C2 extent decrease is mainly due to the continuously disappearance of the C2 waters along the coast of Spain and in the Tyrrhenian Sea. C3 extent decrease is associated with the attenuation of deep-water formation events which has been observed in the Gulf of Lyon since 2013 (Margirier et al., 2020; Prieur et al., 2020).

We observe trends on SST comprised between 0.030°C ± 0.014 and 0.048°C ± 0.014 per year showing a warming of the Mediterranean Sea surface waters. It has been reported in many studies that the water temperature in the Mediterranean Sea has been rising at quite a high rate during the last two decades (Bethoux and Gentili, 1996; Durrieu de Madron et al., 2011), mirroring the global ocean tendency (Levitus et al., 2005). Similar warming trends were observed in remote sensing data, In situ data and model simulations (Herrmann et al., 2008; Mariotti & Dell'aquila, 2012; Marullo et al., 2007, 2011; Nykjaer, 2009; Pisano et al., 2020; Skliris et al., 2012; Vargas-Yáñez et al., 2002, 2008) and warming rates of the Mediterranean basin differ geographically (Nykjaer, 2009; Pisano et al., 2020; Rixen et al., 2005).

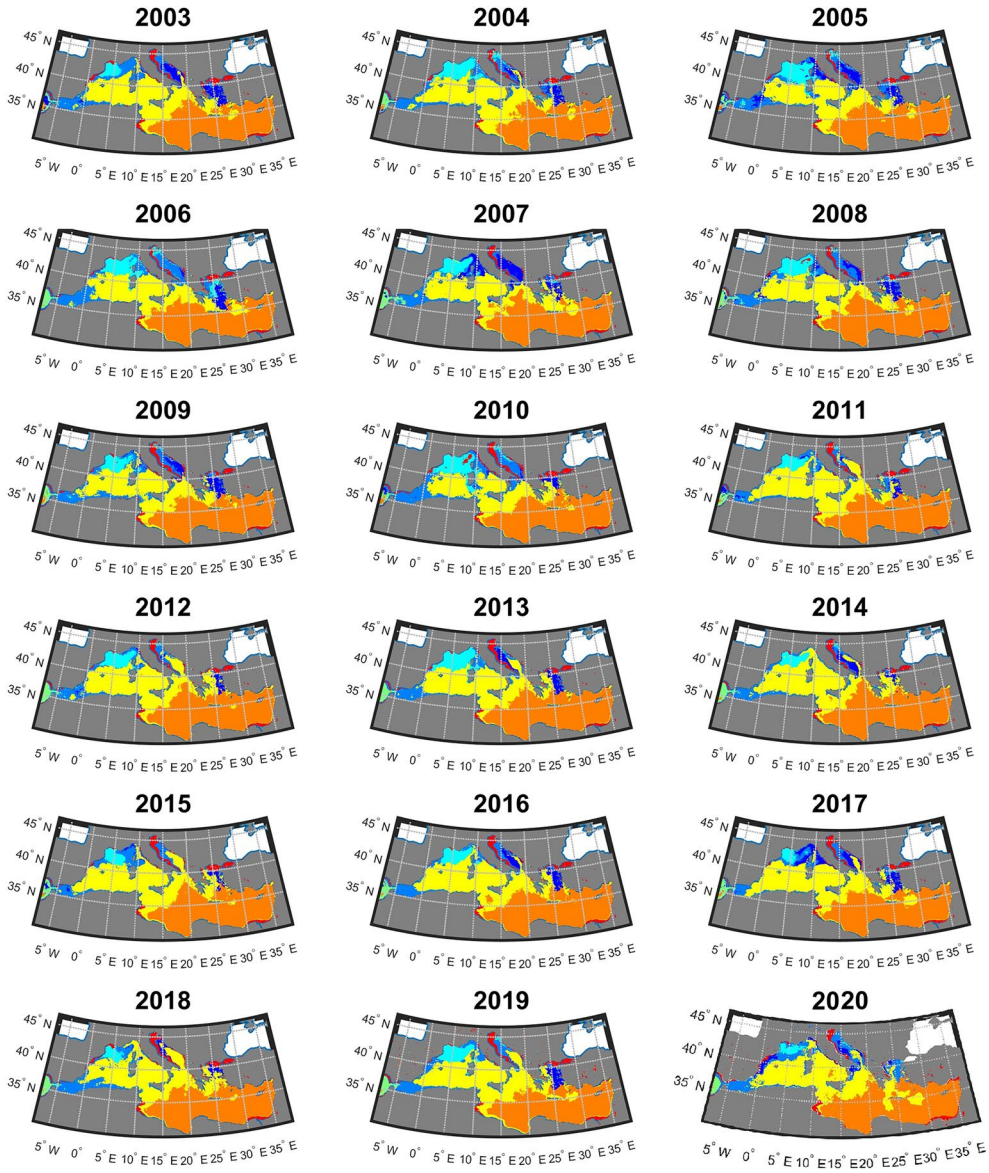

Figure 7. Interannual variability of the extent of the seven bioregions.

Atmospheric temperature oscillations have been proposed as a probable cause of these warming trends in the Mediterranean water temperature (Lelieveld et al., 2002; Marullo et al., 2007). Among these climate variability modes, North Atlantic Oscillation and Atlantic Multidecadal Oscillation (AMO) are particularly relevant for triggering the Mediterranean climate (Pisano et al., 2020). Macias et al. (2013) found that the SST trend of the Med is consistent with the warming phase of the AMO. This coincidence was observed until 2007 and then disappears with the onset of the decreasing phase of AMO, which is not seen in the Mediterranean SST evolution as outlines by Pisano et al. (2020). These remarks support that the continuous increase of the Mediterranean SST is mainly due to global warming at long time scale as it is found for the global ocean (Cazenave et al., 2018). Internal climate variability as AMO can modulate the SST trend at short time scale (decade) but is not responsible for long time scale (several decades) trends.

Meanwhile, negative, yet non-significant trends were observed in this study for each Chla's bioregions and are associated with a strong yearly variability as shown in Figure 8.

Table 4
Yearly Trends in Surface Extents, SST and Chla Concentration of the Different Bioregions

Slope	Surf (%)/yr	SST (°C)/yr	Chla (mg m^{-3})/yr
C1	−0.18 ± 0.11	0.048[b] ± 0.014	0.0002 ± 0.0006
C2	−0.19[a] ± 0.09	0.036[b] ± 0.008	−0.0005 ± 0.0014
C3	−0.19[a] ± 0.09	0.030[a] ± 0.014	−0.0015 ± 0.0018
C4	0.021 ± 0.01	0.001 ± 0.009	−0.0007 ± 0.0019
C5	0.36[a] ± 0.14	0.034[b] ± 0.009	−0.0001 ± 0.0006
C6	0.48[a] ± 0.09	0.038[b] ± 0.009	−0.0002 ± 0.0003
C7	−0.18 ± 0.03	0.023 ± 0.013	−0.0048 ± 0.009

Abbreviations: Chla, chlorophyll-*a*; SST, Sea Surface Temperature.
[a]significant at 5%. [b]significant at 1%.

7. Interannual Variability and Trend of Phytoplankton Composition in the Mediterranean Bioregions

El Hourany, Abboud-Abi Saab, Faour, Aumont, et al. (2019) proposed a methodology (SOM-phytoplankton functional type [PFT]) to identify phytoplankton groups (phytoplankton functional type i.e., PFT) in the Mediterranean Sea from satellite ocean color measurements. This method is based on phytoplankton pigment estimation. Six groups have been identified: Haptophytes, Chlorophytes, Cryptophytes, *Synechococcus*, *Prochlorococcus* and Diatoms. We therefore applied the SOM-PFT method on weekly satellite images of ocean color and SST between 1998 and 2020 to identify the dominant PFT in each bioregion. For each 4 × 4 km satellite pixel, we determined the dominant phytoplankton group. We then allocated a dominant phytoplankton community structure to each bioregion by computing the percentage of satellite pixels assigned to each phytoplankton group. For the seven bioregions, a monthly PFT climatology was calculated (Figure 9), which are presented as PFT percentages, alongside of the 1998–2020 time series illustrated in Figure 10.

The phytoplankton community in the open waters of the Mediterranean Sea is dominated by nanophytoplankton types such as Haptophytes and Chlorophytes in winter and *Synechococcus* in summer (El Hourany, Abboud-Abi Saab, Faour, Mejia, et al., 2019; Navarro et al., 2014, 2017). This is seen in the different

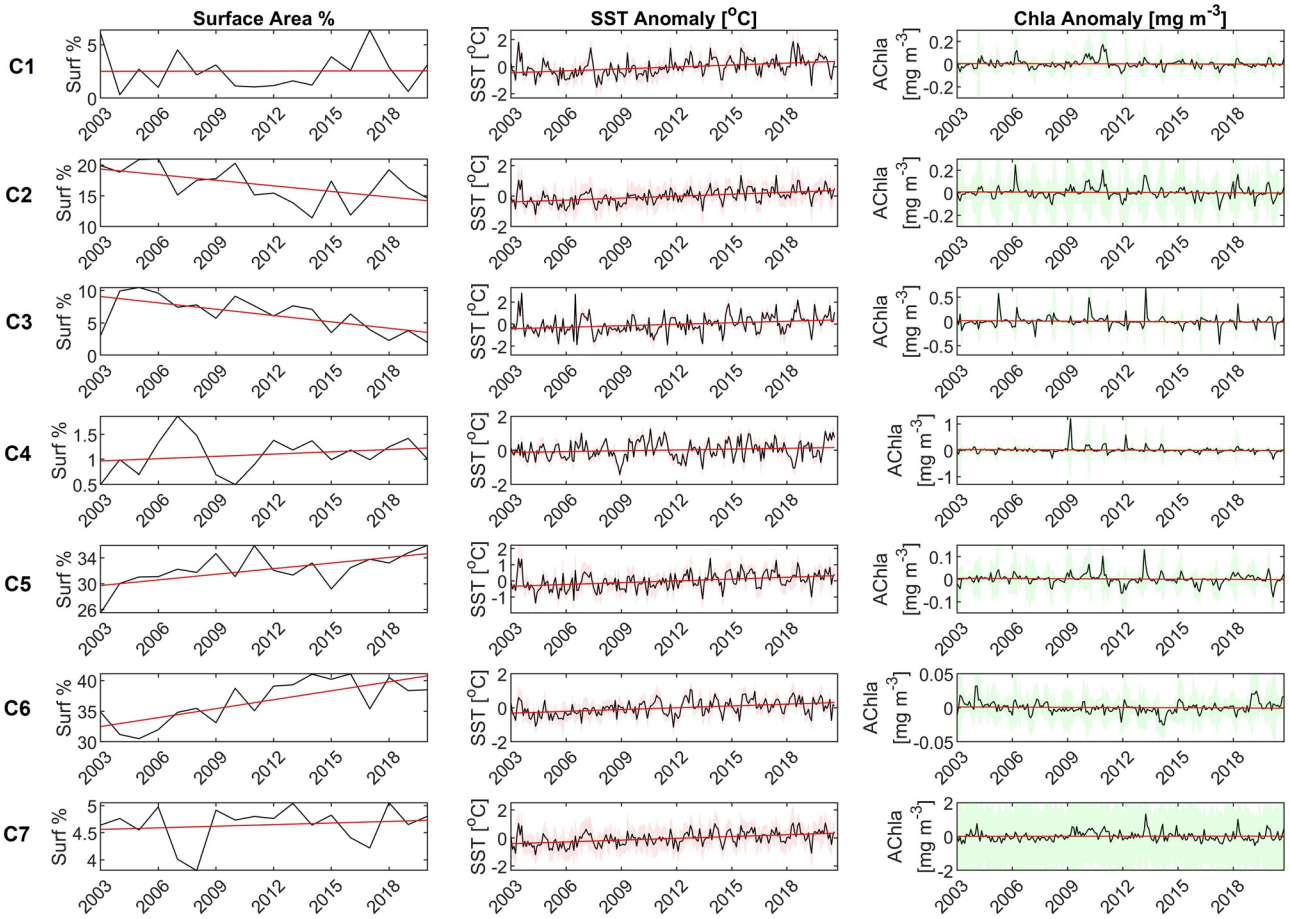

Figure 8. Interannual variability and trend analysis of the geophysical characteristics of the seven bioregions.

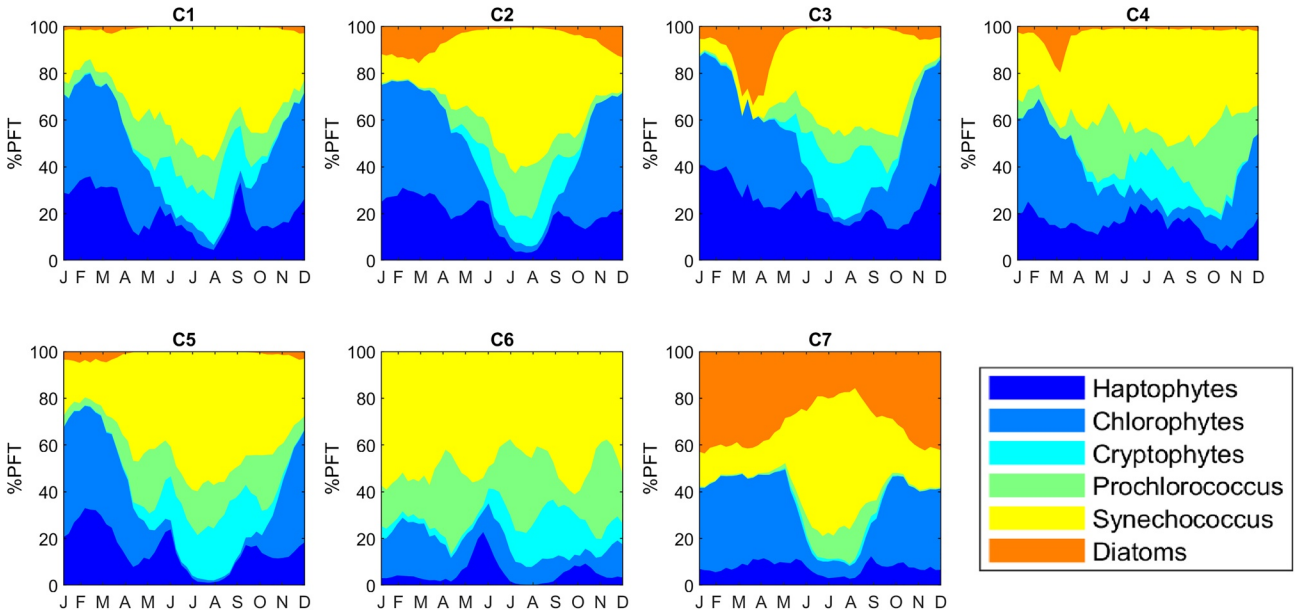

Figure 9. Monthly climatology of the percentage of phytoplankton groups nanophytoplankton (haptophytes, chlorophytes, cryptophytes); picophytoplankton (*Prochlorococcus, Synechoccocus*); Diatoms for the 7 Mediterranean bioregions.

open water bioregions C1, C2, C5, and C6. As for C3, it is directly influenced by the deep winter convection that enriches the surface waters with nutrients (Margirier et al., 2020; Prieur et al., 2020). It results abrupt diatom blooms in late winter (February–March), coinciding with the end of deep convection (Navarro et al., 2017). In coastal bioregions (C7), diatoms tend to dominate in winter and spring, and this is due to the important availability of nutrient from terrigenous input throughout rivers and anthropogenic activity. Figure 10 highlights the PFT weekly variability for the whole studied period for the seven bioregions. We note well-marked seasonal cycles with an interannual variability. This can be associated with several physical and biogeochemical drivers, which can trigger or inhibit the evolution of phytoplankton communities. The study of the mechanisms driving this variability should deserve a full dedicated study.

In El Hourany, Abboud-Abi Saab, Faour, Aumont, et al., 2019, the different sub-basins of the Mediterranean Sea were characterized in terms of PFT variability. This partition was based on the geographical delimitations of the Mediterranean sub-basins. However, comparing this PFT distribution at sub-basins scale, with the PFT distribution observed in the proposed bioregionalization is not straight-forward.

Since physical and biogeochemical gradients can be observed at sub-basin scale, it may result in an occurrence of several bioregions within a sub-basin. As an example, the Adriatic sub-basin is partitioned into four Bioregions, C7, C2, C1, and C5. In other cases, adjacent sub-basins represent a continuum, and therefore share a same bioregion, such as the Levantine and the Ionian Sea sharing bioregion C6. At last, some bioregions are encountered in different sub-basins separated geographically, such as C2 in the Adriatic and the Aegean basins and C7 representing the coastal regions. This occurrence can be explained by similarity in the physical and biogeochemical variability found in some parts of these sub-basins.

Di Cicco et al. (2017), Marty et al. (2002), Organelli et al. (2013), and Sammartino et al. (2015) analyzed algal pigment content and ocean color data to explore the relative contribution of different taxa to total phytoplankton biomass in the Mediterranean Sea. These authors found that spring blooms were dominated by diatoms, while stratifying conditions favor the development of nanophytoplankton, which are then replaced by cyanobacteria (picophytoplankton). The two latter phytoplankton size classes can be considered as markers of oligotrophic conditions, while microphytoplankton (diatoms) are opportunistic and burst after nutrient replenishment. Over the year, nanophytoplankton account for 43%–50% of the total primary production of the Mediterranean Sea, which is largely dominated by Haptophytes (Uitz et al., 2012). Using

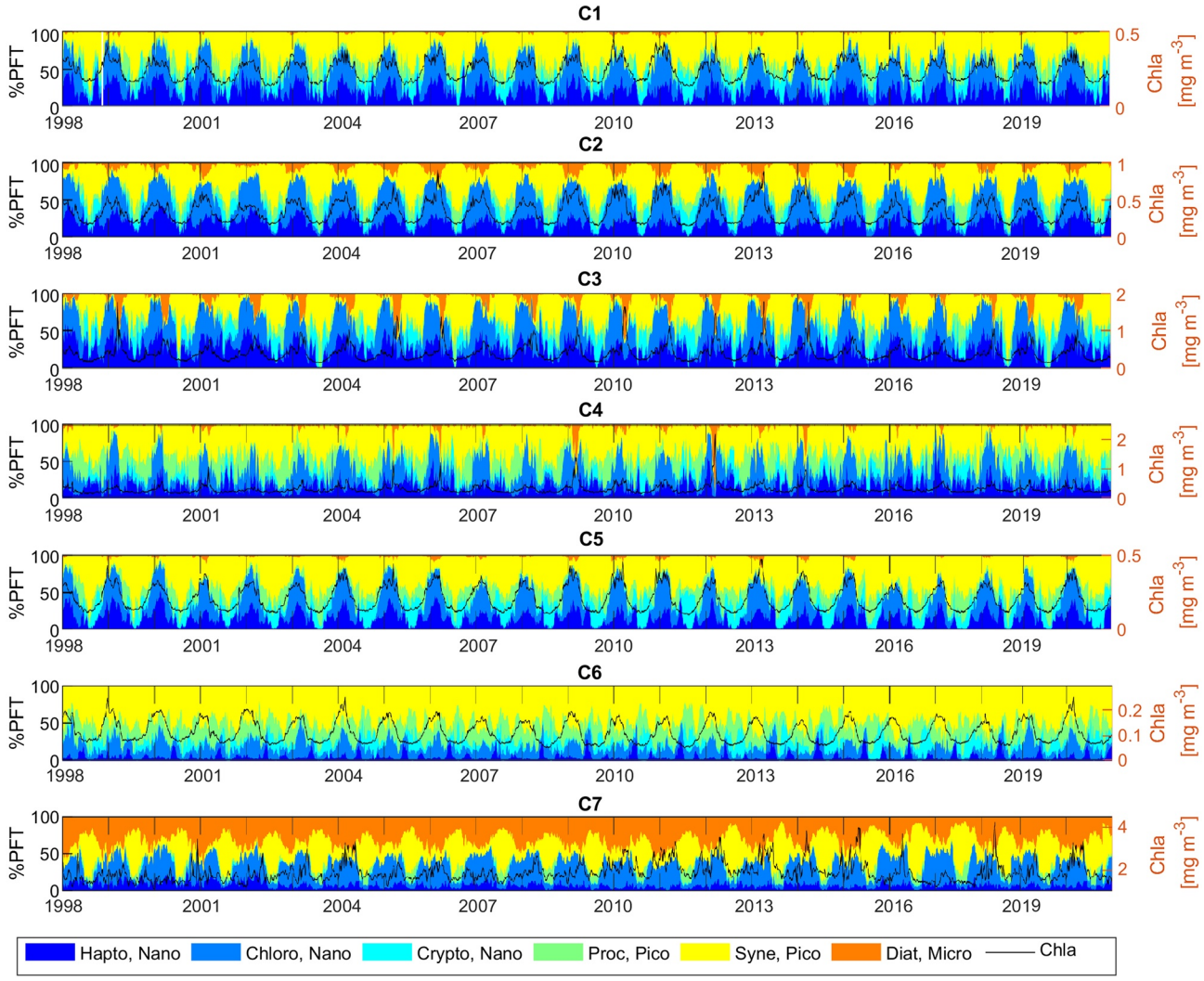

Figure 10. Weekly variability of the percentage of each phytoplankton group nanophytoplankton (haptophytes, chlorophytes, cryptophytes); picophytoplankton (*Prochlorococcus, Synechoccocus*); Diatoms with respect to Chla (dashed line on the right) between 1998 and 2020 in each of the Mediterranean Bioregions.

the method developed in (El Hourany, Abboud-Abi Saab, Faour, Mejia, et al., 2019), we found a similar phytoplankton variability pattern.

The Mediterranean Sea appears to be a host to diverse phytoplankton communities responding to forcing variability differently according to the bioregion (Figures 9 and 10). Studying phytoplankton variability in such a manner highlights the impact of small changes in the physical conditions on these communities. Since bioregions are evidently showing annual trends of extent variability, along with the increase of surface SST, we chose to estimate the annual trends of the satellite-derived PFT communities calculated for each bioregion between 1998 and 2020. In the same way as SST and Chla, we calculated the trends by subtracting the monthly climatology to the monthly PFT values. Then a linear fit model was performed to estimate the yearly trend. The significance of the trends was evaluated using a Mann-Kendall test.

While the Chla concentration does not present any significant trend for this period, Haptophytes exhibited negative yearly trends varying between −0.17% ± 0.07 and −0.41% ± 0.13 in every bioregion except in C6, Chlorophytes increase by 0.5% ± 0.09 yearly in C3 and decrease in C5 and C6 by −0.3% ± 0.09, Cryptophytes increase by around 0.18% ± 0.06 yearly in C5, C6 and C7, while Diatoms decrease with yearly trends varying between 0.18% ± 0.04 and 1.1% ± 0.51 in C1, C2, C3, and C7 and last, Synechococcus exhibit a major increase

Table 5
PFT Yearly Trends in % for the Different Bioregions

	Hapto(%)	Chloro(%)	Crypto(%)	Proc(%)	Syn(%)	Diat(%)
C1	−0.235[b] ± 0.05	0.046 ± 0.05	0.055 ± 0.04	0.043 ± 0.03	0.415[b] ± 0.06	−0.325[b] ± 0.06
C2	−0.243[b] ± 0.09	0.088 ± 0.10	0.081 ± 0.05	−0.003 ± 0.02	0.409[b] ± 0.08	−0.333[b] ± 0.05
C3	−0.167[a] ± 0.07	0.515[b] ± 0.09	0.017 ± 0.07	−0.007 ± 0.01	0.737[b] ± 0.11	−1.094[b] ± 0.51
C4	−0.409[b] ± 0.13	−0.050 ± 0.06	0.029 ± 0.02	−0.012 ± 0.02	0.512[b] ± 0.09	−0.070 ± 0.03
C5	−0.195[a] ± 0.07	−0.326[b] ± 0.07	0.204[b] ± 0.06	0.024 ± 0.01	0.303[b] ± 0.06	−0.010 ± 0.009
C6	−0.017 ± 0.05	−0.315[b] ± 0.09	0.172[b] ± 0.07	−0.007 ± 0.01	0.164[a] ± 0.02	0.003 ± 0.006
C7	−0.229[b] ± 0.06	−0.053 ± 0.06	0.172[b] ± 0.04	0.006 ± 0.005	0.285[b] ± 0.05	−0.182[b] ± 0.04

Abbreviation: PFT, phytoplankton functional type.
[a]significant at 5%. [b]significant at 1%.

in each bioregion with yearly trends between 0.16% ± 0.02 and 0.73% ± 0.11. For the first time, we were able to show that SST warming impacts the phytoplanktonic community in the Mediterranean Sea. We observed a noticeable temperature increase in the surface layers of the Sea and surprisingly a constant Chla concentration over the studied period. The machine learning method in (El Hourany, Abboud-Abi Saab, Faour, Mejia, et al., 2019) allowed us to evidence a noticeable change in the PFT community composition so that Diatom and haptophyte dominations are replaced by Cyanobacteria development. The most affected bioregions by the diatom decrease are the marginal ones (C1, C2, C3, and C7). As for C5, which covers the most important part of the western Mediterranean Sea, presents a decrease of haptophytes and Chlorophytes, which are replaced by Cyanobacteria. The PFT composition of C6 which covers a major part of the eastern Mediterranean Sea changes little because Chlorophyte whose relative decrease is significant (see Table 5) represents a small percentage of this composition (See Figure 4). A reason of these decreases in diatoms and haptophytes is the increase of stratification due the warming of surface waters which blocks the exchanges with the deeper waters. The nutrient enrichment of surface layers is stopped, which increases their oligotrophy. In such nutrient-poor conditions, cyanobacteria are more adapted to strive. Due to global warming, the Mediterranean Sea as a whole (except C7) seems to converge towards an eastern Mediterranean state.

Several multidecadal in situ surveys have been conducted in the Mediterranean Sea (Berline et al., 2012), which evidenced strong seasonal patterns in phytoplankton communities (Ribera d'Alcalà et al., 2004). In the Gulf of Naples, a time series ranging from 1984 to 2000 revealed an over decadal decrease in phytoplankton (Ribera d'Alcalà et al., 2004). Later Mazzocchi et al. (2011) evidenced phytoplankton community changes in the Mediterranean using the same time series. These authors showed that the high production season was becoming shorter and was starting earlier in the year resulting with a decrease in phytoplankton biomass. Using satellite data for the 1998–2009 period (Colella et al., 2016), found heterogeneously distributed Chla trends. However, at a much bigger scale, a decline in total phytoplankton population has been observed in Northern hemisphere basins over the last decade (Gregg & Rousseaux, 2014) and is projected to strengthen over the 21st century over wide oceanic regions under all global warming scenarios (Kwiatkowski et al., 2020). This decline is one of the consequences of climate change, as highlighted by recent IPCC reports (IPCC-SROCC-Pörtner et al., 2019).

8. Conclusion

The 2S-SOM-Med allowed us to obtain a well differentiated classification of the Mediterranean Sea waters by clustering seasonal cycles of monthly climatological values of Chla, SST, and MLD. These classes can be considered as bioregions governed by specific physical and biogeochemical processes. The classification identified seven distinct bioregions.

C5 and C6 occupy the largest surface of the Mediterranean Sea. C5 characterizes the offshore waters of the western basin and is influenced by hydrodynamic processes which govern this basin, such as advection of Atlantic water, which causes phytoplankton to proliferate due to nutrients in surface water. C6 extends from the center of the Mediterranean basin to the eastern coasts and is characterized by oligo-trophic wa-

ters associated with high SST. The extent of these two bioregions is quite stable from one year to another except the Rhodes gyre area characterized by C5 which is very variable C1 waters characterize the Aegean Sea and the Adriatic Sea, which are both intermediate and deep-water formation places. C2 is found in several disconnected regions which are governed by large surface currents. C3 is confined to the Ligurian and Balearic seas; it is characterized by deep winter convection phenomena, which enriches this region with nutrients from the deep layers, causing a significant phytoplankton blooms at the end of winter. This bioregion shrinks during the studied period due to a decrease of deep-water formation. C4 characterizes the Atlantic water. At last, C7 waters have the highest Chla concentration due to their location (coastal areas, discharge of important rivers such as Nil, Po, Rhone, Ebro, shallow shelfs with quite important tides facilitating the presence of suspended matters); C7 waters are probably case-2 waters.

We then showed that it is possible to refine this decomposition by analyzing the significance of the neurons constituting the seven classes. This was applied with success to the neurons of C2, which is a bioregion encountered in geographically disconnected regions of the Mediterranean Sea. We were able to break down C2 into subclasses, each of them corresponding to a well identified water mass associated with a dedicated neuron of the 2S-SOM classifier. The regionalization of every neuron proves that the 2S-SOM-Med has efficiently differentiated these waters without the addition of any complementary parameter. We found in few specific cases, it should be necessary to add salinity as an explanatory variable, but most of the bioregions evidenced in the present and past studies can be identified with the three variables we used (satellite SST and Chla, and MLD).

The variability of the phytoplankton groups estimated by the El Hourany, Abboud-Abi Saab, Faour, Aumont, et al. (2019) method allowed us to better characterize the bioregions. The dominance of the nanophytoplankton groups is largely observed in the western basin (C3 and C5 regions) from autumn to spring. While the dominance of different types of the cyanobacteria *Synechococcus* and *Prochlorococcus* is highlighted in summer and more precisely in the waters of the C6 bioregion of the eastern basin. Diatoms dominate throughout the year in the C7-marked coastal and shallow regions, which can be explained by the continuous higher availability of inorganic nutrient originating from terrigenous input. Diatoms also largely benefit from the strong deep convection in the C3 bioregion marked by a large bloom at the end of winter convection in March.

At last, we were able to evidence an interesting behavior of the biomass of the Mediterranean Sea under SST warming whose long-term trend can be attributed to climate change (Cazenave et al., 2018; Somot et al., 2006, 2008). Although the surface layers are becoming warmer the total biomass stays constant during the studied period. But we were able to evidence a noticeable change in the estimated phytoplankton community composition; diatoms and haptophytes dominance are replaced by cyanobacteria development. The Mediterranean Sea is shifting to an Eastern Mediterranean state.

Data Availability Statement

The MODIS Aqua Sea Surface Temperature and Chlorophyll-*a* data were obtained from the NASA ocean color website (https://oceandata.sci.gsfc.nasa.gov/MODIS-Aqua). The Mixed-Layer Depth Climatology was acquired from http://mixedlayer.ucsd.edu/. Data and codes are publicly available at https://github.com/RoyElHourany/MEDBioregion_2S-SOM; 2S-SOM algorithm can be found at https://gitlab.in2p3.fr/carlos.mejia/2S-SOM_versionCM; the SOM algorithm for PFT retrieval is available at https://github.com/RoyElHourany/SOM-Pigments.

Acknowledgment
This work was funded by the GDRI O-LiFE observatory, the Lebanese National Council for the Scientific Research (CNRS-L) and the Hubert Curien Program CEDRE 2020–2021 (No. 44536NL). This work was also supported by the CNES-TOSCA project 2018/2019. R. El Hourany's work is funded by the CNES postdoctoral grant 2019.

References

Armi, Z., Trabelsi, E., Turki, S., Béjaoui, B., & MaïzBen (2010). Seasonal phytoplankton responses to environmental factors in a shallow Mediterranean lagoon. *Journal of Marine Science and Technology*, *15*(4), 417–426. https://doi.org/10.1007/s00773-010-0093-y

Ayata, S.-D., Irisson, J.-O., Aubert, A., Berline, L., Dutay, J.-C., Mayot, N., et al. (2018). Regionalisation of the Mediterranean basin, a MERMEX synthesis. *Progress in Oceanography*, *163*, 7–20. https://doi.org/10.1016/j.pocean.2017.09.016

Badran, F., Yacoub, M., & Thiria, S. (2005). Self-organizing maps and unsupervised classification. In *Neural Networks: Methodology and Applications (Neural net)*. Springer Berlin Heidelberg. https://doi.org/10.1007/3-540-28847-3_7

Basterretxea, G., Font-Muñoz, J. S., Salgado-Hernanz, P. M., Arrieta, J., & Hernández-Carrasco, I. (2018). Patterns of chlorophyll interannual variability in Mediterranean biogeographical regions. *Remote Sensing of Environment*, *215*, 7–17. https://doi.org/10.1016/j.rse.2018.05.027

Berline, L., Rammou, A.-M., Doglioli, A., Molcard, A., & Petrenko, A. (2014). A connectivity-based eco-regionalization method of the Mediterranean Sea. *PloS One*, *9*(11), e111978. https://doi.org/10.1371/journal.pone.0111978

Berline, L., Siokou-Frangou, I., Marasović, I., Vidjak, O., Fernández de Puelles, M. L., Mazzocchi, M. G., et al. (2012). Intercomparison of six Mediterranean zooplankton time series. *Progress in Oceanography*, *97–100*, 76–91. https://doi.org/10.1016/j.pocean.2011.11.011

Bethoux, J. P., & Gentili, B. (1996). The Mediterranean Sea, coastal and deep-sea signatures of climatic and environmental changes. *Journal of Marine Systems*, *7*(2), 383–394. http://doga.ogs.trieste.it/doga/echo/eo/pdf/1996Bethoux_gentili.pdf

Bethoux, J. P., Gentili, B., Morin, P., Nicolas, E., Pierre, C., & Ruiz-Pino, D. P. (1999). The Mediterranean Sea: A miniature ocean for climatic and environmental studies and a key for the climatic functioning of the North Atlantic. *Progress in Oceanography*, *44*(1–3), 131–146. https://doi.org/10.1016/S0079-6611(99)00023-3

Bethoux, J. P., Gentili, B., Raunet, J., & Tailliez, D. (1990). Warming trend in the western Mediterranean deep water. *Nature*, *347*(6294), 660–662. https://doi.org/10.1038/347660a0

Campbell, J. W., & Feng, H. (2005). *The empirical chlorophyll algorithm for MODIS: Testing the OC3M algorithm using NOMAD data*. University of New Hampshire.

Cazenave, A., Palanisamy, H., & Ablain, M. (2018). Contemporary sea level changes from satellite altimetry: What have we learned? What are the new challenges? *Advances in Space Research*, *62*(7), 1639–1653. https://doi.org/10.1016/j.asr.2018.07.017

Colella, S., Falcini, F., Rinaldi, E., Sammartino, M., & Santoleri, R. (2016). Mediterranean ocean colour chlorophyll trends. *PloS One*, *11*(6). https://doi.org/10.1371/journal.pone.0155756

Coll, M., Piroddi, C., Steenbeek, J., Kaschner, K., Ben Rais Lasram, F., Aguzzi, J., et al. (2010). The biodiversity of the Mediterranean Sea: Estimates, patterns, and threats. *PloS One*, *5*(8), e11842. https://doi.org/10.1371/journal.pone.0011842

Di Cicco, A., Sammartino, M., Marullo, S., & Santoleri, R. (2017). Regional empirical algorithms for an improved identification of phytoplankton functional types and size classes in the Mediterranean Sea using satellite data. *Frontiers in Marine Science*, *4*(126). https://doi.org/10.3389/fmars.2017.00126

D'Ortenzio, F., & Ribera d'Alcalà, M. (2008). On the trophic regimes of the Mediterranean Sea: A satellite analysis. *Biogeosciences Discussions*, *5*(4), 2959–2983. https://doi.org/10.5194/bgd-5-2959-2008

D'Ortenzio, F., & Ribera d'Alcalà, M. (2009). On the trophic regimes of the Mediterranean Sea: A satellite analysis. *Biogeosciences*, *6*(2), 139–148. https://doi.org/10.5194/bg-6-139-2009

D'Ortenzio, F., Taillandier, V., Claustre, H., Prieur, L. M., Leymarie, E., Mignot, A., et al. (2020). Biogeochemical Argo: The test case of the NAOS Mediterranean Array. *Frontiers in Marine Science*, *7*(120). https://doi.org/10.3389/fmars.2020.00120

d'Ovidio, F., Fernández, V., Hernández-García, E., & López, C. (2004). Mixing structures in the Mediterranean Sea from finite-size Lyapunov exponents. *Geophysical Research Letters*, *31*(17). https://doi.org/10.1029/2004GL020328

Durrieu de Madron, X., Guieu, C., Sempéré, R., Conan, P., Cossa, D., D'Ortenzio, F., et al. (2011). Marine ecosystems' responses to climatic and anthropogenic forcings in the Mediterranean. *Progress in Oceanography*, *91*(2), 97–166. https://doi.org/10.1016/j.pocean.2011.02.003

El Hourany, R., Abboud-Abi Saab, M., Faour, G., Aumont, O., Crépon, M., & Thiria, S. (2019). Estimation of secondary phytoplankton pigments from satellite observations using self-organizing maps (SOM). *Journal of Geophysical Research: Oceans*, *124*, 1357–1378. https://doi.org/10.1029/2018JC014450

El Hourany, R., Abboud-Abi Saab, M., Faour, G., Mejia, C., Crépon, M., & Thiria, S. (2019). Phytoplankton diversity in the Mediterranean Sea from satellite data using self-organizing maps. *Journal of Geophysical Research: Oceans*, *124*, 5827–5843. https://doi.org/10.1029/2019JC015131

El Hourany, R., Fadel, A., Gemayel, E., Abboud-Abi Saab, M., & Faour, G. (2017). Spatio-temporal variability of the phytoplankton biomass in the Levantine basin between 2002 and 2015 using MODIS products. *Oceanologia*, *59*(2). https://doi.org/10.1016/j.oceano.2016.12.002

Farikou, O., Sawadogo, S., Niang, A., Diouf, D., Brajard, J., Mejia, C., et al. (2015). Inferring the seasonal evolution of phytoplankton groups in the Senegalo-Mauritanian upwelling region from satellite ocean-color spectral measurements. *Journal of Geophysical Research: Oceans*, *120*, 6581–6601. https://doi.org/10.1002/2015JC010738

Ferrara, R., & Maserti, B. E. (1992). Mercury concentration in the water, particulate matter, plankton and sediment of the Adriatic Sea. *Marine Chemistry*, *38*(3–4), 237–249. https://doi.org/10.1016/0304-4203(92)90036-A

Foukal, N. P., & Thomas, A. C. (2014). Biogeography and phenology of satellite-measured phytoplankton seasonality in the California current. *Deep-Sea Research Part I: Oceanographic Research Papers*, *92*, 11–25. https://doi.org/10.1016/j.dsr.2014.06.008

Giorgi, F. (2006). Climate change hot-spots. *Geophysical Research Letters*, *33*(8), L08707. https://doi.org/10.1029/2006GL025734

Gregg, W. W., & Rousseaux, C. S. (2014). Decadal trends in global pelagic ocean chlorophyll: A new assessment integrating multiple satellites, in situ data, and models. *Journal of Geophysical Research: Oceans*, *119*, 5921–5933. https://doi.org/10.1002/2014JC010158

Herrmann, M., Estournel, C., Déqué, M., Marsaleix, P., Sevault, F., & Somot, S. (2008). Dense water formation in the Gulf of Lions shelf: Impact of atmospheric interannual variability and climate change. *Continental Shelf Research*, *28*(15), 2092–2112. https://doi.org/10.1016/j.csr.2008.03.003

Holte, J., & Talley, L. (2009). A new algorithm for finding mixed layer depths with applications to Argo data and Subantarctic mode water formation*. *Journal of Atmospheric and Oceanic Technology*, *26*(9), 1920–1939. https://doi.org/10.1175/2009JTECHO543.1

Holte, J., Talley, L. D., Gilson, J., & Roemmich, D. (2017). An Argo mixed layer climatology and database. *Geophysical Research Letters*, *44*(11), 5618–5626. https://doi.org/10.1002/2017GL073426

Hu, C., Lee, Z., & Franz, B. (2012). Chlorophyll-*a* algorithms for oligotrophic oceans: A novel approach based on three-band reflectance difference. *Journal of Geophysical Research*, *117*. https://doi.org/10.1029/2011JC007395

Jain, A. K., & Dubes, R. C. (1988). *Algorithms for clustering data*. Prentice-Hall, Inc. https://dl.acm.org/doi/abs/10.5555/46712

Jouini, M., Béranger, K., Arsouze, T., Beuvier, J., Thiria, S., Crépon, M., & Taupier-Letage, I. (2016). The Sicily Channel surface circulation revisited using a neural clustering analysis of a high-resolution simulation. *Journal of Geophysical Research: Oceans*, *121*, 4545–4567. https://doi.org/10.1002/2015JC011472

Jouini, M., Lévy, M., Crépon, M., & Thiria, S. (2013). Reconstruction of satellite chlorophyll images under heavy cloud coverage using a neural classification method. *Remote Sensing of Environment*, *131*, 232–246. https://doi.org/10.1016/j.rse.2012.11.025

Kilpatrick, K. A., Podestá, G., Walsh, S., Williams, E., Halliwell, V., Szczodrak, M., et al. (2015). A decade of sea surface temperature from MODIS. *Remote Sensing of Environment*, *165*, 27–41. https://doi.org/10.1016/j.rse.2015.04.023

Kohonen, T. (2013). Essentials of the self-organizing map. *Neural Networks*, *37*, 52–65. https://doi.org/10.1016/J.NEUNET.2012.09.018

Kwiatkowski, L., Torres, O., Bopp, L., Aumont, O., Chamberlain, M., R. Christian, J., et al. (2020). Twenty-first century ocean warming, acidification, deoxygenation, and upper-ocean nutrient and primary production decline from CMIP6 model projections. *Biogeosciences*, *17*(13), 3439–3470. https://doi.org/10.5194/bg-17-3439-2020

Lavender, S. J., Moufaddal, W. M., & Pradhan, Y. D. (2009). Assessment of temporal shifts of chlorophyll levels in the Egyptian Mediterranean shelf and satellite detection of the Nile bloom. *Egyptian Journal of Aquatic Research*, *35*(2), 121–135.

Lejeusne, C., Chevaldonné, P., Pergent-Martini, C., Boudouresque, C. F., & Pérez, T. (2010). Climate change effects on a miniature ocean: The highly diverse, highly impacted Mediterranean Sea. In *Trends in Ecology and evolution* (Vol. *25*(4), pp. 250–260). Elsevier Current Trends. https://doi.org/10.1016/j.tree.2009.10.009

Lelieveld, J., Berresheim, H., Borrmann, S., Crutzen, P. J., Dentener, F. J., Fischer, H., et al. (2002). Global air pollution crossroads over the Mediterranean. *Science*, *298*(5594), 794–799. https://doi.org/10.1126/science.1075457

Levitus, S., Antonov, J., & Boyer, T. (2005). Warming of the world ocean, 1955–2003. *Geophysical Research Letters*, *32*(2), 1–4. https://doi.org/10.1029/2004GL021592

Liu, Y., & Weisberg, R. H. (2005). Patterns of ocean current variability on the West Florida Shelf using the self-organizing map. *Journal of Geophysical Research*, *110*(C6), C06003. https://doi.org/10.1029/2004JC002786

Liu, Y., Weisberg, R. H., & Mooers, C. N. K. (2006). Performance evaluation of the self-organizing map for feature extraction. *Journal of Geophysical Research*, *111*(C5), C05018. https://doi.org/10.1029/2005JC003117

Longhurst, A. (1998). *Ecological geography of the sea*. Academic Press.

Longhurst, A., Sathyendranath, S., Platt, T., & Caverhill, C. (1995). An estimate of global primary production in the ocean from satellite radiometer data. *Journal of Plankton Research*, *17*(6), 1245–1271. https://doi.org/10.1093/plankt/17.6.1245

López García, M. J., & Camarasa, B. A. M. (2011). Recent trends of SST in the Western Mediterranean basins from AVHRR Pathfinder data (1985–2007). *Global and Planetary Change*, *78*(3–4), 127–136. https://doi.org/10.1016/j.gloplacha.2011.06.001

Macias, D., Garcia-Gorriz, E., & Stips, A. (2013). Understanding the causes of recent warming of Mediterranean Waters. How much could be attributed to climate change? *PloS One*, *8*(11), e81591. https://doi.org/10.1371/journal.pone.0081591

Margirier, F., Testor, P., Heslop, E., Mallil, K., Bosse, A., Houpert, L., et al. (2020). Abrupt warming and salinification of intermediate waters interplays with decline of deep convection in the Northwestern Mediterranean Sea. *Scientific Reports*, *10*(1), 1–11. https://doi.org/10.1038/s41598-020-77859-5

Mariotti, A., & Dell'aquila, A. (2012). Decadal climate variability in the Mediterranean region: Roles of large-scale forcings and regional processes. *Springer*, *38*(5–6), 1129–1145. https://doi.org/10.1007/s00382-011-1056-7

Marty, J.-C., Chiavérini, J., Pizay, M.-D., & Avril, B. (2002). Seasonal and interannual dynamics of nutrients and phytoplankton pigments in the western Mediterranean Sea at the DYFAMED time-series station (1991–1999). *Deep Sea Research Part II: Topical Studies in Oceanography*, *49*(11), 1965–1985. https://doi.org/10.1016/S0967-0645(02)00022-X

Marullo, S., Artale, V., & Santoleri, R. (2011). The SST multidecadal variability in the Atlantic-Mediterranean region and its relation to AMO. *Journal of Climate*, *24*(16), 4385–4401. https://doi.org/10.1175/2011JCLI3884.1

Marullo, S., Nardelli, B. B., Guarracino, M., & Santoleri, R. (2007). Observing the Mediterranean Sea from space: 21 years of Pathfinder-AVHRR sea surface temperatures (1985 to 2005): Re-analysis and validation. *Ocean Science*, *3*(2), 299–310. https://doi.org/10.5194/os-3-299-2007

Mayot, N., Ortenzio, F. D., Ribera, M., Lavigne, H., Claustre, H., Biologica, O., et al. (2016). *Interannual variability of the Mediterranean trophic regimes from ocean color satellites* (pp. 1901–1917). https://doi.org/10.5194/bg-13-1901-2016

Mazzocchi, M. G., Licandro, P., Dubroca, L., Di Capua, I., & Saggiomo, V. (2011). Zooplankton associations in a Mediterranean long-term time-series. *Journal of Plankton Research*, *33*(8), 1163–1181. https://doi.org/10.1093/plankt/fbr017

McCall, J. (2008). Primary production and marine fisheries associated with the Nile outflow. *Earth and Environment*, *2893*, 179–208. http://homepages.see.leeds.ac.uk/~lecac/ejournal/3,179-208.pdf

Mignot, J., Mejia, C., Sorror, C., Sylla, A., Crépon, M., & Thiria, S. (2020). Towards an objective assessment of climate multi-model ensembles – a case study: The Senegalo-Mauritanian upwelling region. *Geoscientific Model Development*, *13*(6), 2723–2742. https://doi.org/10.5194/gmd-13-2723-2020

Navarro, G., Almaraz, P., Caballero, I., Vázquez, Á., & Huertas, I. E. (2017). Reproduction of spatio-temporal patterns of major Mediterranean phytoplankton groups from remote sensing OC-CCI data. *Frontiers in Marine Science*, *4*(August), 1–16. https://doi.org/10.3389/fmars.2017.00246

Navarro, G., Alvain, S., Vantrepotte, V., & Huertas, I. E. (2014). Identification of dominant phytoplankton functional types in the Mediterranean Sea based on a regionalized remote sensing approach. *Remote Sensing of Environment*, *152*(February 2016), 557–575. https://doi.org/10.1016/j.rse.2014.06.029

Niang, A., Badran, F., Moulin, C., Crépon, M., & Thiria, S. (2006). Retrieval of aerosol type and optical thickness over the Mediterranean from SeaWiFS images using an automatic neural classification method. *Remote Sensing of Environment*, *100*(1), 82–94. https://doi.org/10.1016/J.RSE.2005.10.005

Niang, A., Gross, L., Thiria, S., Badran, F., & Moulin, C. (2003). Automatic neural classification of ocean colour reflectance spectra at the top of the atmosphere with introduction of expert knowledge. *Remote Sensing of Environment*, *86*(2), 257–271. https://doi.org/10.1016/S0034-4257(03)00113-5

Nieblas, A.-E., Drushka, K., Reygondeau, G., Rossi, V., Demarcq, H., Dubroca, L., & Bonhommeau, S. (2014). Defining Mediterranean and Black Sea biogeochemical subprovinces and synthetic ocean indicators using mesoscale oceanographic features. *PloS One*, *9*(10), e111251. https://doi.org/10.1371/journal.pone.0111251

Nykjaer, L. (2009). Mediterranean Sea surface warming 1985–2006. *Climate Research*, *39*(1), 11–17. https://doi.org/10.3354/cr00794

Organelli, E., Bricaud, A., Antoine, D., & Uitz, J. (2013). Multivariate approach for the retrieval of phytoplankton size structure from measured light absorption spectra in the Mediterranean Sea (BOUSSOLE site). *Applied Optics*, *52*(11), 2257–2273. https://doi.org/10.1364/AO.52.002257

Outtara, M. (2014). *Développement et mise en place d'une méthode de classification multi-blocs: Application aux données de l'OQAI*. Conservatoire national des arts et metiers – CNAM. Retrieved from https://tel.archives-ouvertes.fr/tel-01062782/

Palmiéri, J. (2014). Modélisation biogéochimique de la mer Méditerranée avec le modèle régional couplé NEMO-MED12/PISCES. In *Sciences de la Terre*. Université de Versailles-Saint Quentin en Yvelines.

Pisano, A., Marullo, S., Artale, V., Falcini, F., Yang, C., Leonelli, F. E., et al. (2020). New evidence of Mediterranean climate change and variability from Sea Surface Temperature observations. *Remote Sensing*, *12*(1), 132. https://doi.org/10.3390/RS12010132

Pörtner, H.-O., Roberts, D. C., Masson-Delmotte, V., Zhai, P., Tignor, M., Poloczanska, E., et al. (2019). *IPCC Special Report on the Ocean and Cryosphere in a changing climate*. Retrieved from https://www.ipcc.ch/srocc/chapter/summary-for-policymakers/

Prieur, L., D'ortenzio, F., Taillandier, V., & Testor, P. (2020). Physical Oceanography of the Ligurian Sea. In *The Mediterranean Sea in the Era of Global Change 1* (pp. 49–78). Wiley. https://doi.org/10.1002/9781119706960.ch3

Raicich, F. (1996). On the fresh water balance of the Adriatic Sea. *Journal of Marine Systems*, *9*(3–4), 305–319. https://doi.org/10.1016/S0924-7963(96)00042-5

Reygondeau, G., Guieu, C., Benedetti, F., Irisson, J.-O., Ayata, S.-D., Gasparini, S., & Koubbi, P. (2017). Biogeochemical regions of the Mediterranean Sea: An objective multidimensional and multivariate environmental approach. *Progress in Oceanography*, *151*, 138–148. https://doi.org/10.1016/J.POCEAN.2016.11.001

Reygondeau, G., Irisson, J.-O., Ayata, S. D., Gasparini, S., Benedetti, F., Albouy, C., et al. (2014). *Definition of the Mediterranean eco-regions and maps of potential pressures in these eco-regions*. Retrieved from http://www.perseus-net.eu/assets/media/PDF/deliverables/3336.6_Final.pdf

Reynolds, R. W., Smith, T. M., Liu, C., Chelton, D. B., Casey, K. S., & Schlax, M. G. (2007). Daily high-resolution-blended analyses for sea surface temperature. *Journal of Climate*, *20*(22), 5473–5496. https://doi.org/10.1175/2007JCLI1824.1

Ribera d'Alcalà, M., Conversano, F., Corato, F., Licandro, P., Mangoni, O., Marino, D., et al. (2004). Seasonal patterns in plankton communities in pluriannual time series at a coastal Mediterranean site (Gulf of Naples): An attempt to discern recurrences and trends. *Scientia Marina*, *68*(SUPPL 1), 65–83. https://doi.org/10.3989/scimar.2004.68s165

Richardson, A. J., Risien, C., & Shillington, F. A. (2003). Using self-organizing maps to identify patterns in satellite imagery. *Progress in Oceanography*, *59*(2–3), 223–239. https://doi.org/10.1016/j.pocean.2003.07.006

Rixen, M., Beckers, J. M., Levitus, S., Antonov, J., Boyer, T., Maillard, C., et al. (2005). The Western Mediterranean Deep Water: A proxy for climate change. *Geophysical Research Letters*, *32*(12), 1–4. https://doi.org/10.1029/2005GL022702

Rossi, V., Ser-Giacomi, E., López, C., & Hernández-García, E. (2014). Hydrodynamic provinces and oceanic connectivity from a transport network help designing marine reserves. *Geophysical Research Letters*, *41*, 2883–2891. https://doi.org/10.1002/2014GL059540

Salem, Z. B., Drira, Z., & Ayadi, H. (2015). What factors drive the variations of phytoplankton, ciliate and mesozooplankton communities in the polluted southern coast of Sfax, Tunisia? *Environmental Science and Pollution Research*, *22*(15), 11764–11780. https://doi.org/10.1007/s11356-015-4416-8

Sammartino, M., Cicco, A. D., Marullo, S., & Santoleri, R. (2015). *Phytoplankton in the Mediterranean Sea from satellite ocean colour data of SeaWiFS* (pp. 759–778). https://doi.org/10.5194/os-11-759-2015

Sawadogo, S., Brajard, J., Niang, A., Lathuiliere, C., Crepon, M., & Thiria, S. (2009). Analysis of the Senegalo-Mauritanian upwelling by processing satellite remote sensing observations with topological maps. In *2009 International Joint Conference on Neural Networks* (pp. 2826–2832). Atlanta, GA. https://doi.org/10.1109/IJCNN.2009.5178623

Shaltout, M., & Omstedt, A. (2014). Recent sea surface temperature trends and future scenarios for the Mediterranean Sea. *Oceanologia*, *56*(3), 411–443. https://doi.org/10.5697/oc.56-3.411

Shata, A., & El Fayoumy, I. (1970). Remarks on the hydrogeology of the Nile delta, UAR. *Hydrology of Deltas*, 385–396.

Skliris, N., Sofianos, S., Gkanasos, A., Mantziafou, A., Vervatis, V., Axaopoulos, P., & Lascaratos, A. (2012). Decadal scale variability of sea surface temperature in the Mediterranean Sea in relation to atmospheric variability. *Ocean Dynamics*, *62*(1), 13–30. https://doi.org/10.1007/s10236-011-0493-5

Somot, S., Houpert, L., Sevault, F., Testor, P., Bosse, A., Taupier-Letage, I., et al. (2018). Characterizing, modelling and understanding the climate variability of the deep water formation in the North-Western Mediterranean Sea. *Climate Dynamics*, *51*(3), 1179–1210. https://doi.org/10.1007/s00382-016-3295-0

Somot, S., Sevault, F., & Déqué, M. (2006). Transient climate change scenario simulation of the Mediterranean Sea for the twenty-first century using a high-resolution ocean circulation model. *Climate Dynamics*, *27*(7–8), 851–879. https://doi.org/10.1007/s00382-006-0167-z

Somot, S., Sevault, F., Déqué, M., & Crepon, M. (2008). 21st century climate change scenario for the Mediterranean using a coupled atmosphere-ocean regional climate model. *Global and Planetary Change*, *63*(2–3), 112–126. https://doi.org/10.1016/j.gloplacha.2007.10.003

Spalding, M. D., Fox, H. E., Allen, G. R., Davidson, N., Ferdaña, Z. A., Finlayson, M., et al. (2007). Marine ecoregions of the world: A bioregionalization of coastal and shelf areas. *Bioscience*, *57*(7), 573–583. https://doi.org/10.1641/b570707

Syvitski, J. P. M., & Saito, Y. (2007). Morphodynamics of deltas under the influence of humans. *Global and Planetary Change*, *57*(3–4), 261–282. https://doi.org/10.1016/J.GLOPLACHA.2006.12.001

Tsiola, A., Pitta, P., Fodelianakis, S., Pete, R., Magiopoulos, I., Mara, P., et al. (2016). Nutrient limitation in surface waters of the oligotrophic. *Microbial Ecology*, *71*(3), 575–588.

Uitz, J., Stramski, D., Gentili, B., D'Ortenzio, F., & Claustre, H. (2012). Estimates of phytoplankton class-specific and total primary production in the Mediterranean Sea from satellite ocean color observations. *Global Biogeochemical Cycles*, *26*(2), 1–10. https://doi.org/10.1029/2011GB004055

Vargas-Yáñez, M., Jesús García, M., Salat, J., García-Martínez, M. C., Pascual, J., & Moya, F. (2008). Warming trends and decadal variability in the Western Mediterranean shelf. *Global and Planetary Change*, *63*(2–3), 177–184. https://doi.org/10.1016/j.gloplacha.2007.09.001

Vargas-Yáñez, M., Plaza, F., García-Lafuente, J., Sarhan, T., Vargas, J., & Vélez-Belchi, P. (2002). About the seasonal variability of the Alboran Sea circulation. *Journal of Marine Systems*, *35*(3–4), 229–248. https://doi.org/10.1016/S0924-7963(02)00128-8

Walton, C. C., Pichel, W. G., Sapper, J. F., & May, D. A. (1998). The development and operational application of nonlinear algorithms for the measurement of sea surface temperatures with the NOAA polar-orbiting environmental satellites. *Journal of Geophysical Research*, *103*(C12), 27999–28012. https://doi.org/10.1029/98JC02370

Wang, X. H., Pinardi, N., & Malacic, V. (2007). Sediment transport and resuspension due to combined motion of wave and current in the northern Adriatic Sea during a Bora event in January 2001: A numerical modelling study. *Continental Shelf Research*, *27*(5), 613–633. https://doi.org/10.1016/j.csr.2006.10.008

Yala, K., Niang, N., Brajard, J., Mejia, C., Ouattara, M., El Hourany, R., et al. (2020). Estimation of phytoplankton pigments from ocean-color satellite observations in the Senegalo-Mauritanian region by using an advanced neural classifier. *Ocean Science*, *16*(2), 513–533. https://doi.org/10.5194/os-16-513-2020

Yoder, J. A., & Kennelly, M. A. (2003). Seasonal and ENSO variability in global ocean phytoplankton chlorophyll derived from 4 years of SeaWiFS measurements. *Global Biogeochemical Cycles*, *17*(4). https://doi.org/10.1029/2002gb001942